Supplement of Geosci. Model Dev., 14, 6273–6289, 2021
https://doi.org/10.5194/gmd-14-6273-2021-supplement

Geoscientific Model Development
Open Access
EGU

Supplement of

A parameterization of sub-grid topographical effects on solar radiation in the E3SM Land Model (version 1.0): implementation and evaluation over the Tibetan Plateau

Dalei Hao et al.

Correspondence to: Dalei Hao (dalei.hao@pnnl.gov)

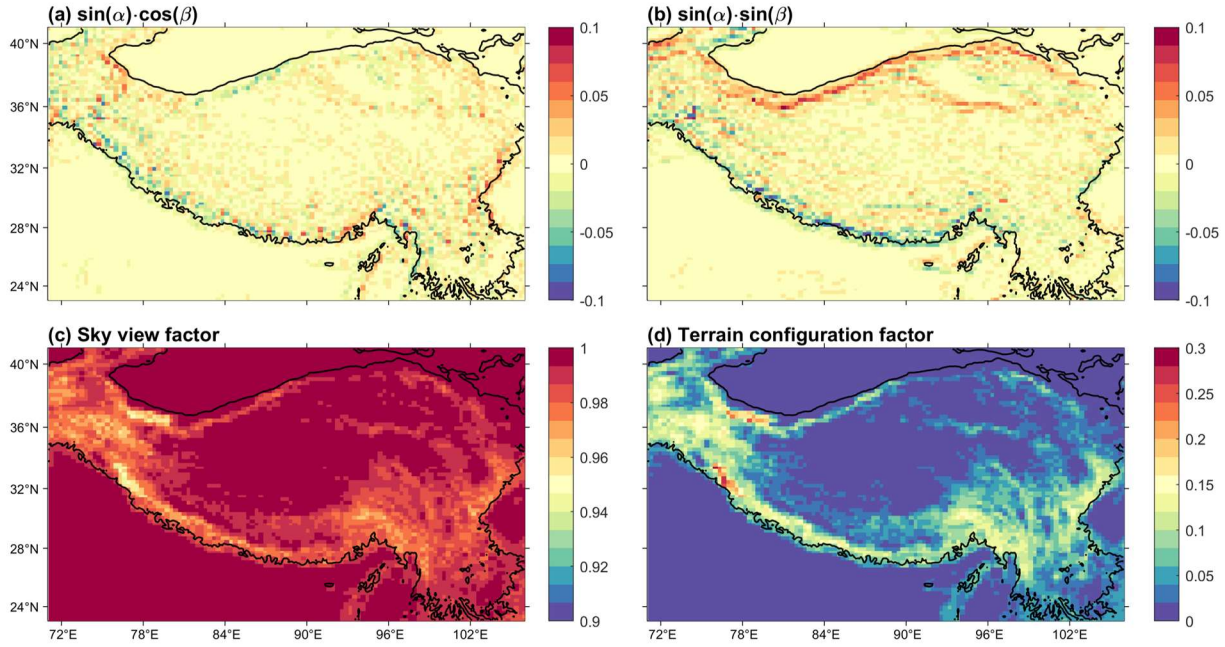

Figure S1. Spatial distributions of grid averaged values of sin(α) · cos(β) (a), sin(α) · sin(β) (b), sky view factor (c) and terrain configuration factor (d) derived from 90 m DEM at 0.125°x0.125° spatial resolution over the TP.

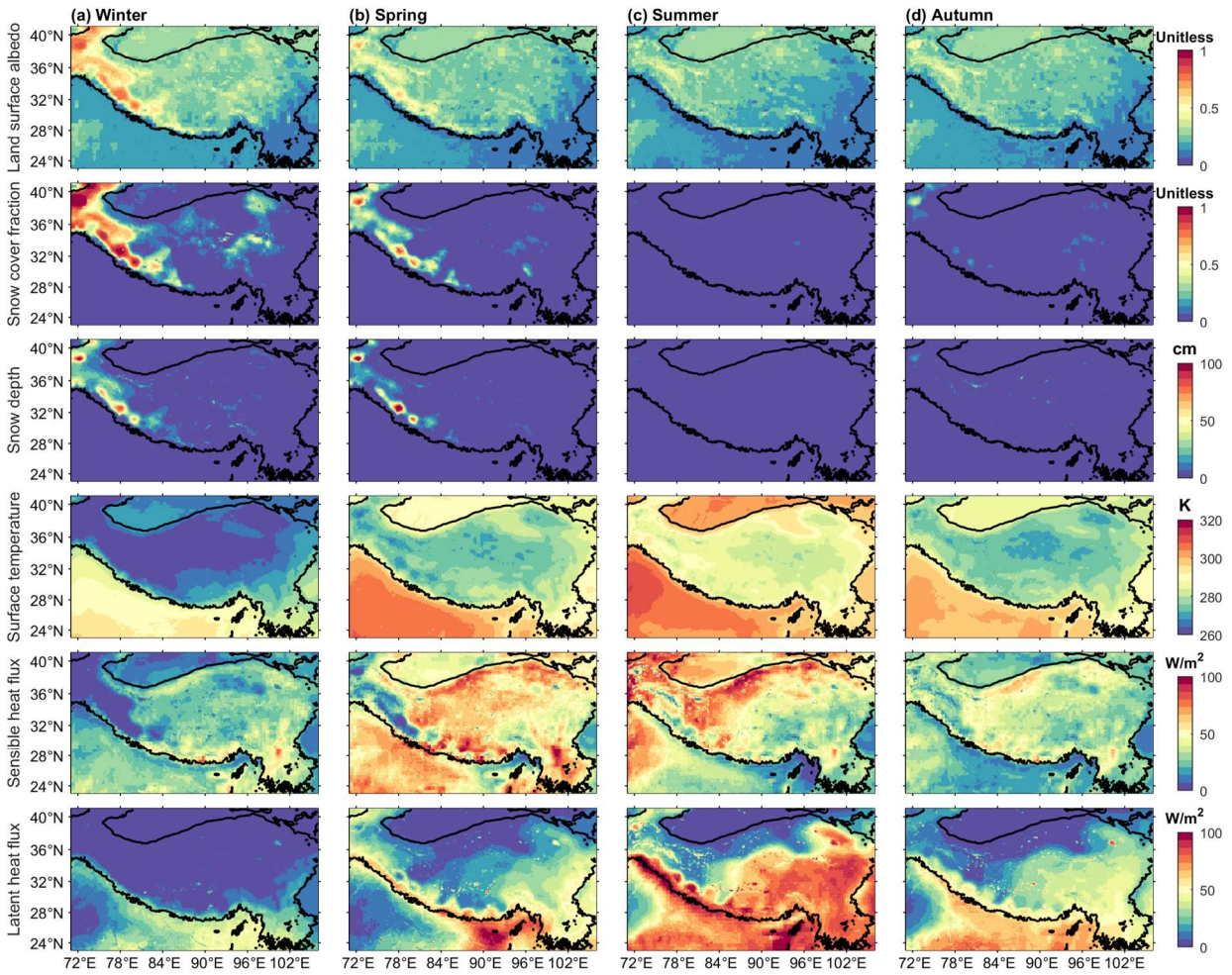

Figure S2. Spatial patterns of PP simulated variables (from top to bottom): land surface albedo, snow cover fraction, snow depth, surface temperature, sensible heat flux and latent heat flux, respectively for different seasons.

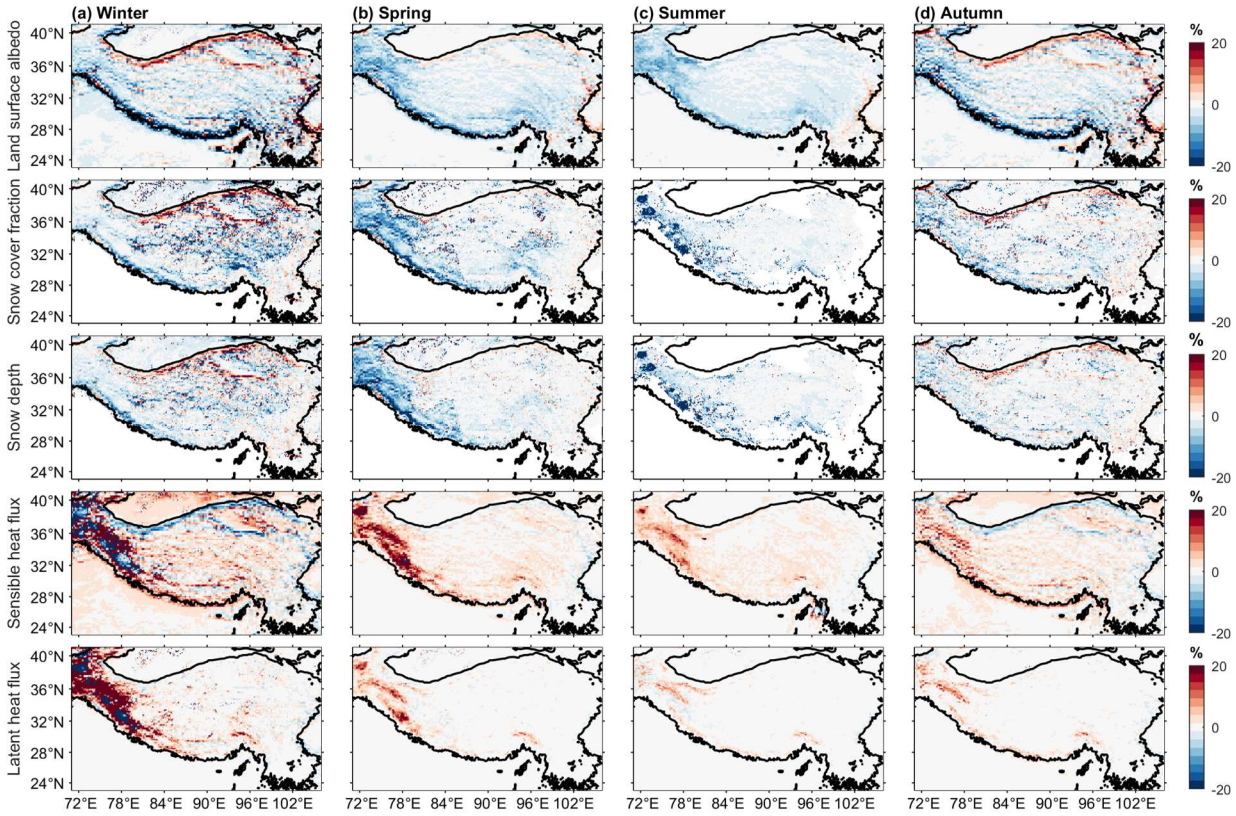

Figure S3. Relative differences between TOP and PP for different seasons in different variables (from top to bottom): land surface albedo, snow cover fraction, snow depth, sensible heat flux and latent heat flux.

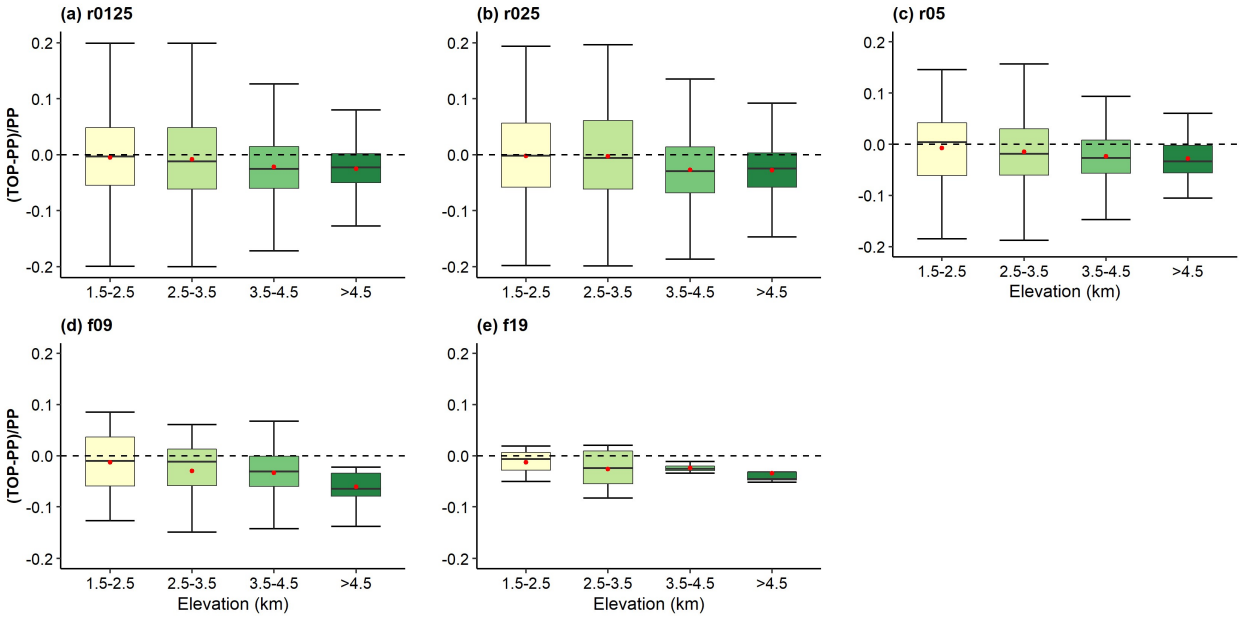

Figure S4. Boxplots of the relative differences in land surface albedo between TOP and PP in winter at different spatial scales and different elevation bands. Red points represent the mean values.

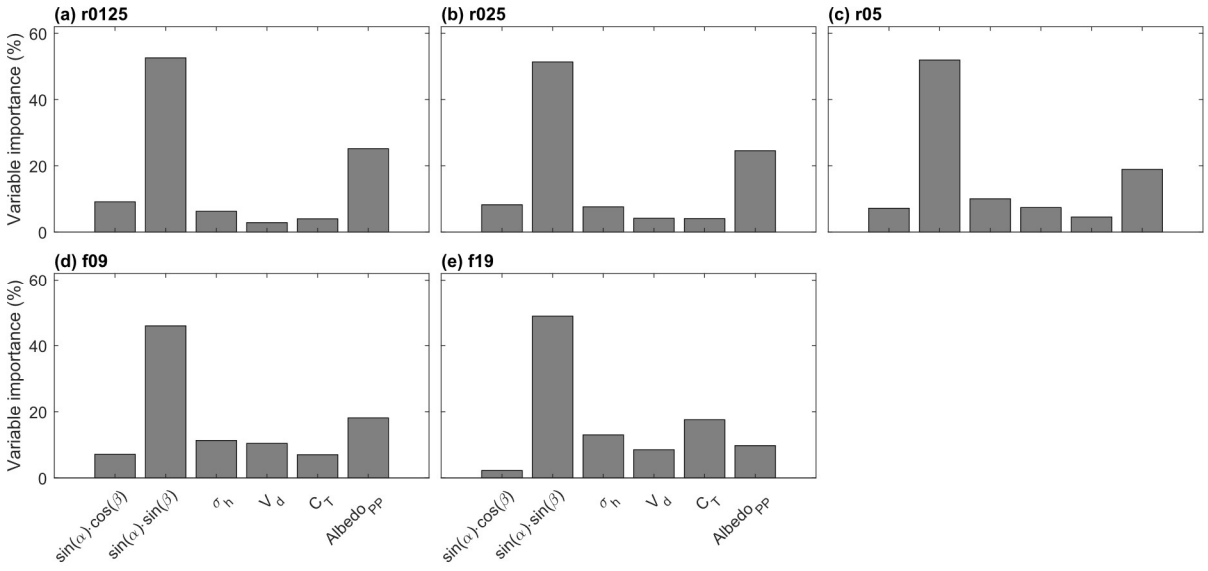

Figure S5. The relative contributions of different factors to the relative difference in land surface albedo between TOP and PP in winter at different spatial scales.

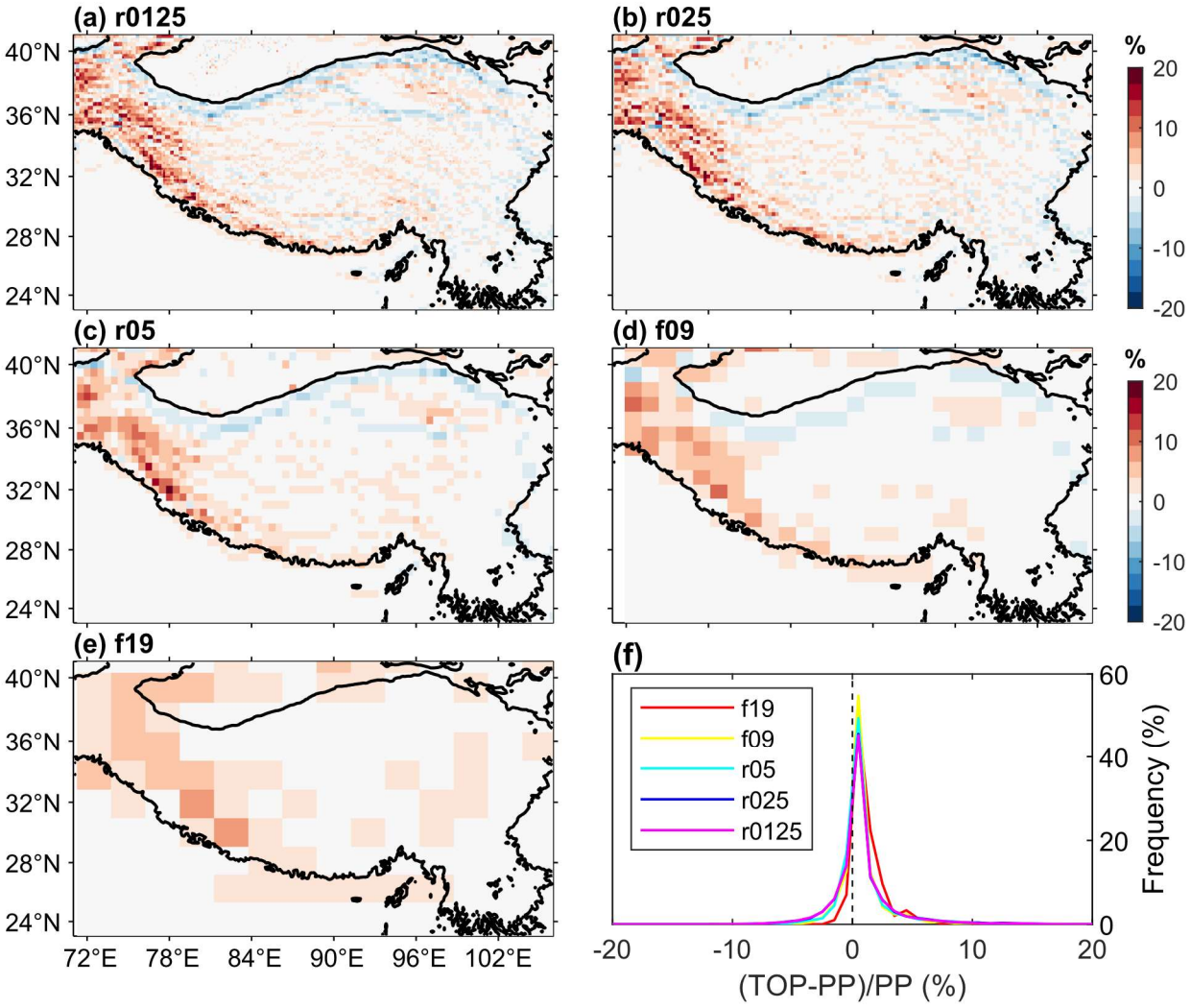

Figure S6. The relative differences in net solar radiation between TOP and PP in winter at different spatial scales (a-e) and the statistical histogram of their frequent distributions (f).

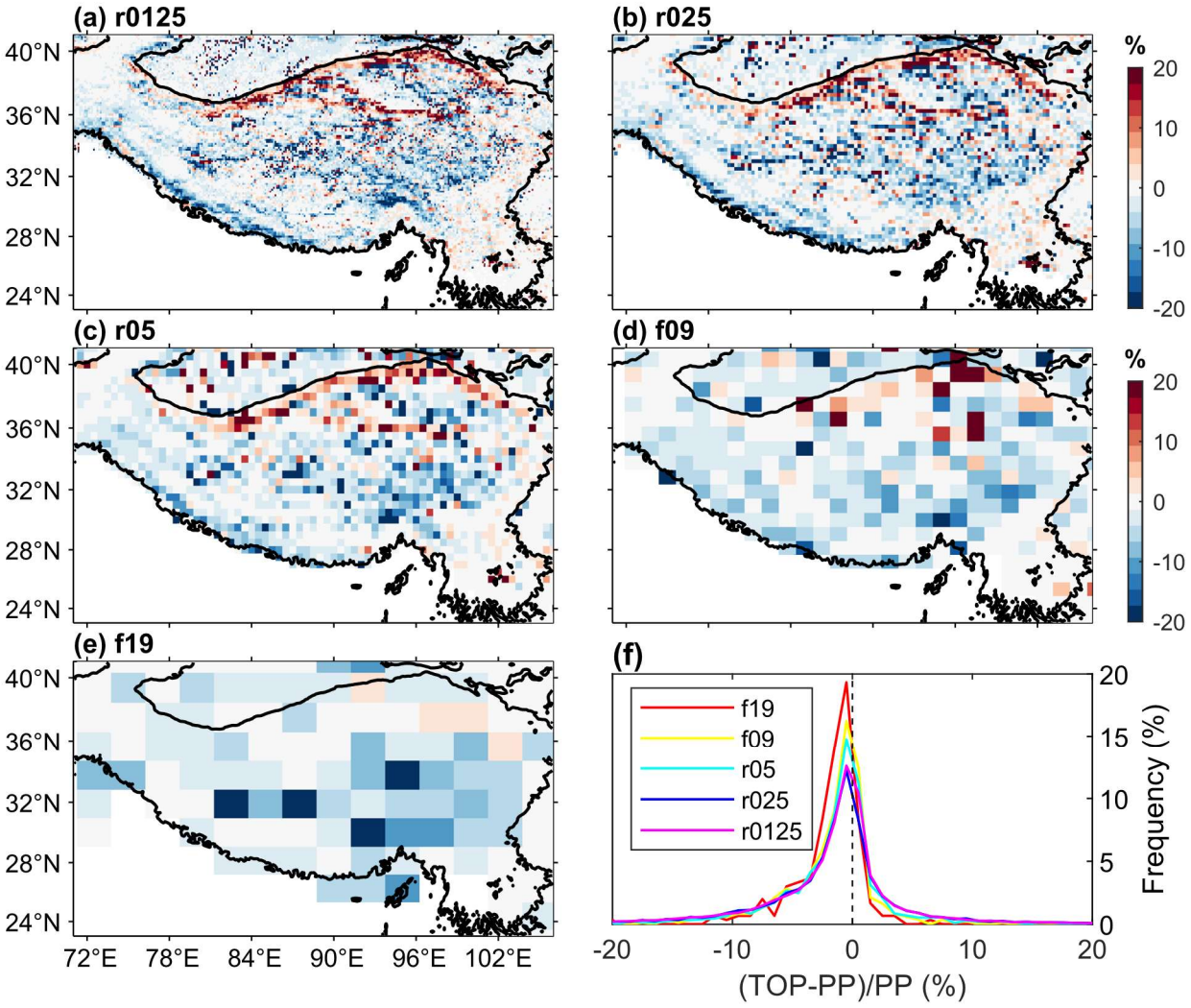

Figure S7. Same as Figure S6 except for snow cover fraction.

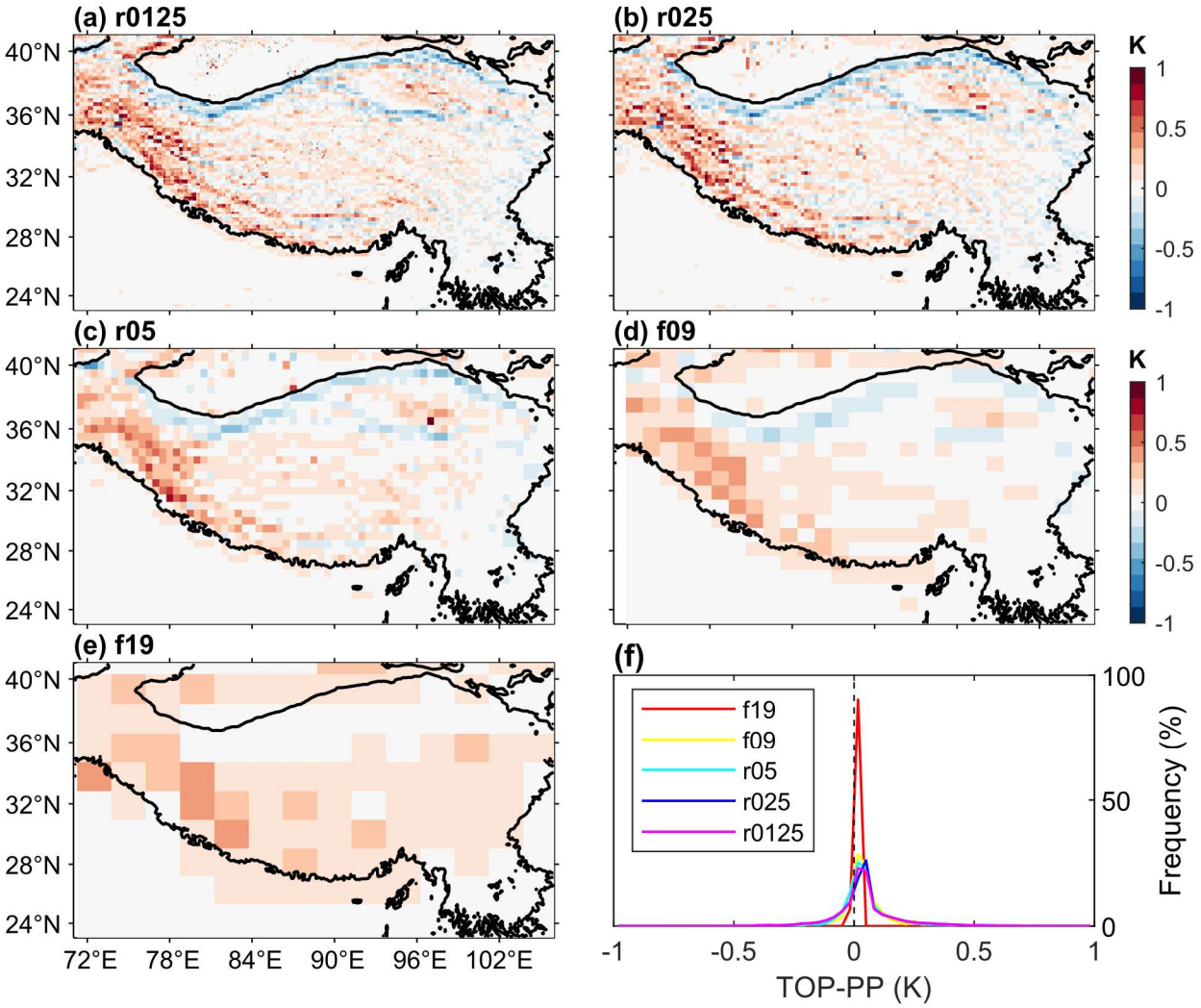

Figure S8. Same as Figure S6 except for the absolute differences of surface temperature.

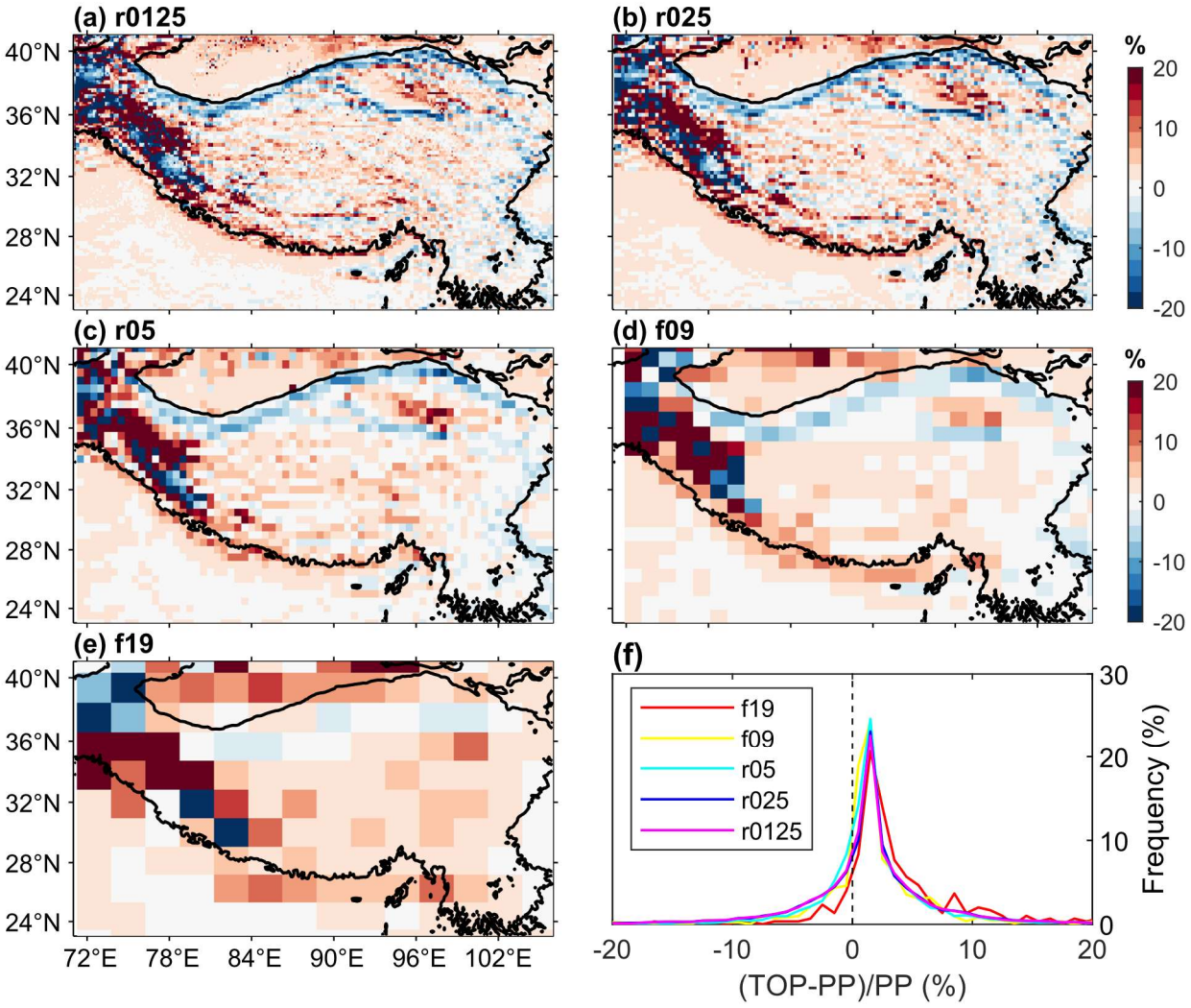

Figure S9. Same as Figure S6 except for sensible heat flux.

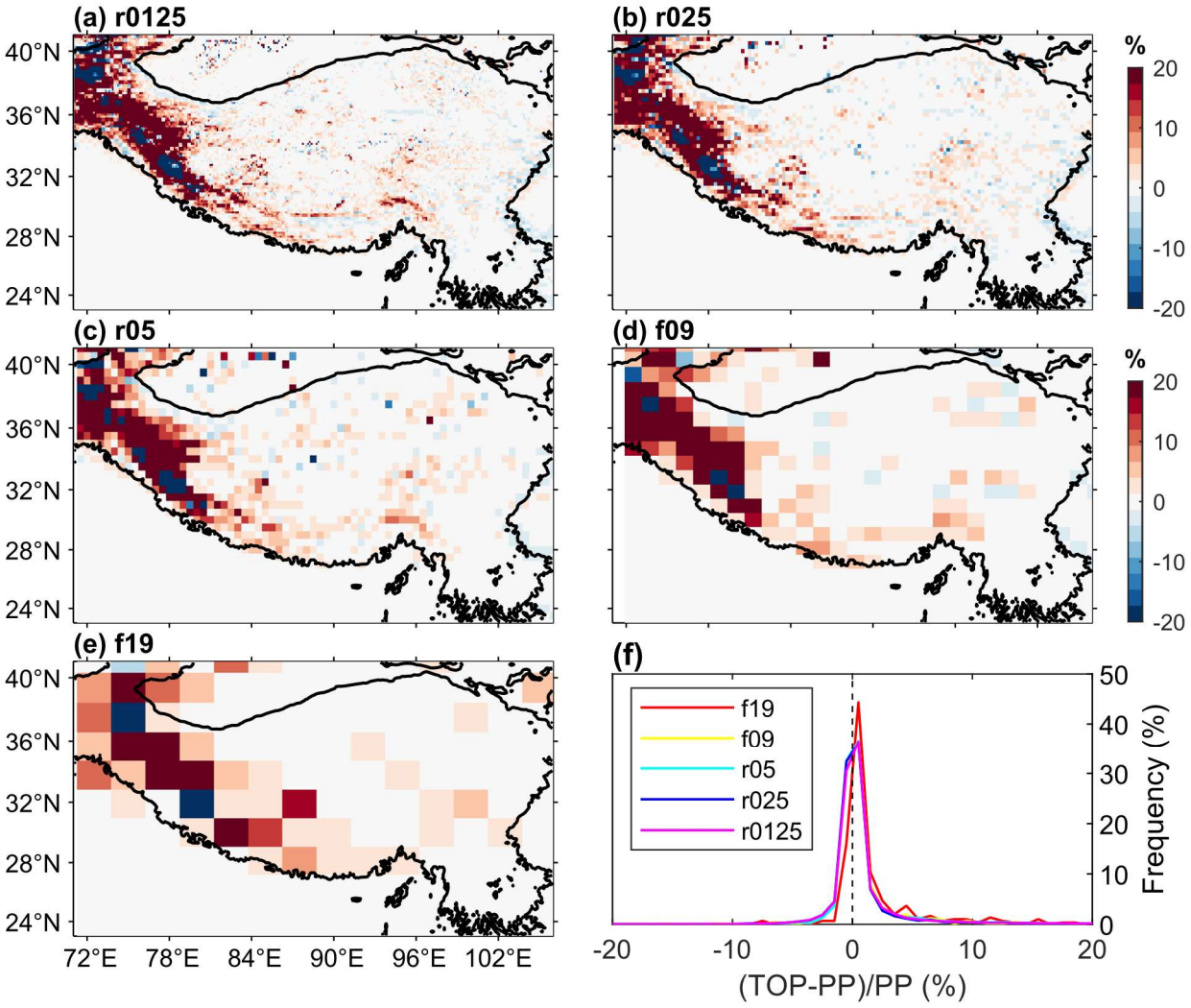

Figure S10. Same as Figure S6 except for latent heat flux.

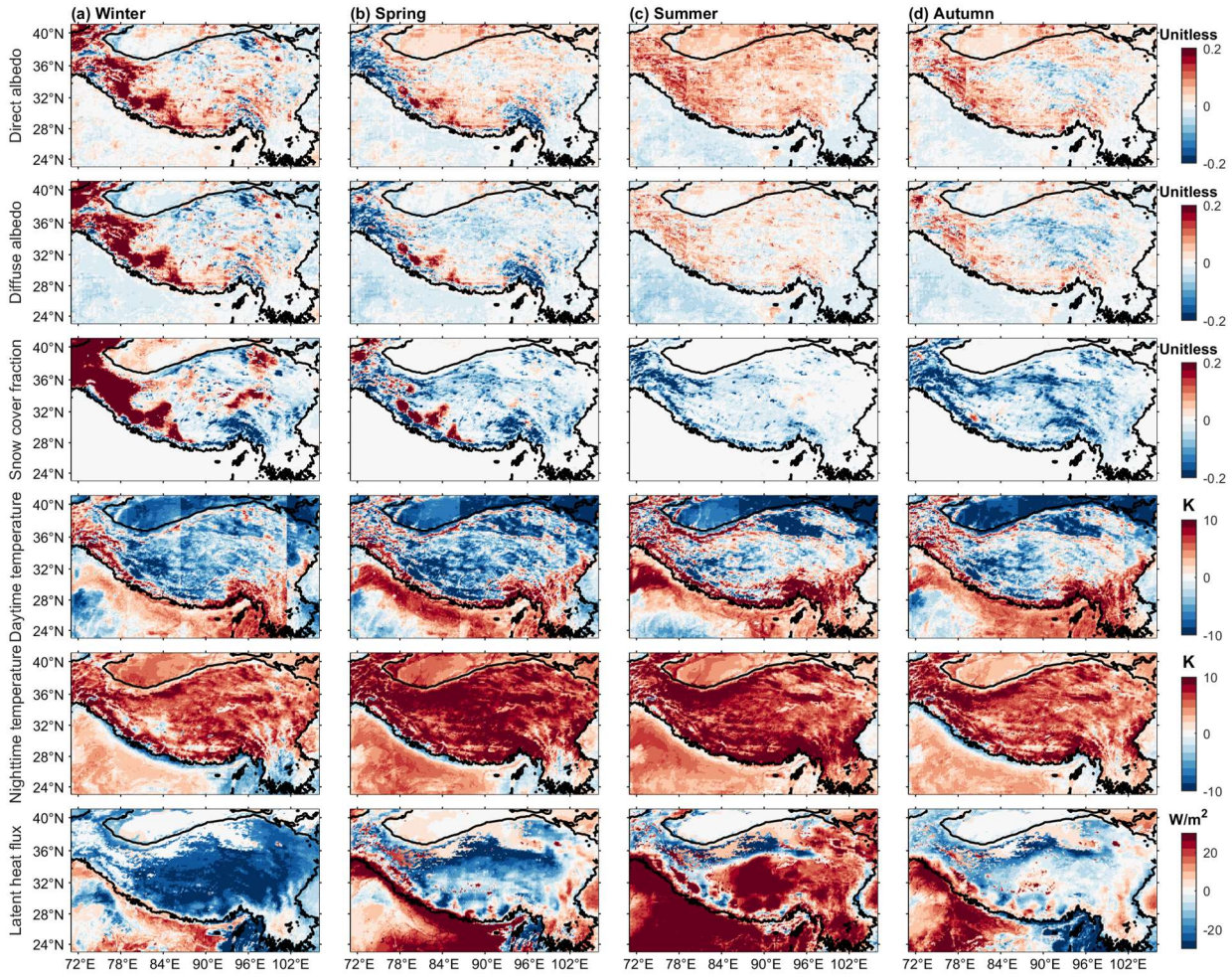

Figure S11. The bias of PP ($|\boldsymbol{\delta}_{PP}|$) with respect to MODIS data for four seasons in different variables (from top to bottom): direct albedo, diffuse albedo, snow cover fraction, daytime and nighttime surface temperature, and latent heat flux.

Table S1. Fitted parameters corresponding to different factors for direct and diffuse flux in equation 5, derived based on the 3D Monte Carlo simulations.

SZA	Direct flux					Diffuse flux				
	$\bar{\mu}$	σ_h	$\overline{V_d}$	$\overline{C_T}$	1	$\bar{\mu}$	σ_h	$\overline{V_d}$	$\overline{C_T}$	1
0.1	6.792×10^{-1}	0	2.045×10	0	-2.103×10	2.456×10^{-2}	3.146×10^{-7}	4.385×10^{0}	0	-4.382×10^{0}
0.25	9.284× 10-1	0	1.993×10^{0}	0	-2.911×10^{0}	5.606×10^{-2}	6.001×10^{-7}	4.068×10^{0}	0	-4.085×10^{0}
0.4	9.863×10^{-1}	0	5.900×10^{-2}	0	-1.045×10^{-0}	1.049×10^{-1}	7.436×10^{-7}	3.911×10^{0}	0	-3.960×10^{0}
0.55	9.942×10^{-1}	0	5.270×10^{-3}	0	-9.995×10^{-1}	1.734×10^{-1}	7.806×10^{-7}	3.763×10^{0}	0	-3.863×10^{0}
0.70	9.959×10^{-1}	0	2.977×10^{-3}	0	-9.990×10^{-1}	2.543×10^{-1}	7.581×10^{-7}	3.559×10^{0}	0	-3.727×10^{0}
0.85	9.959×10^{-1}	0	2.977×10^{-3}	0	-9.990×10^{-1}	0	7.015×10^{-7}	3.298×10^{0}	0	-3.547×10^{0}
1.00	0	0	8.347×10^{-3}	0	-8.393×10^{-3}	2.456×10^{-2}	6.359×10^{-7}	2.984×10^{0}	0	-2.984×10^{0}

Table S2. Fitted parameters corresponding to different factors for direct-reflected and diffuse-reflected flux in equation 5, derived based on the 3D Monte Carlo simulations.

SZA	Direct-reflected flux					Diffuse-reflected flux				
	$\bar{\mu}$	σ_h	$\overline{V_d}$	$\overline{C_T}$	1	$\bar{\mu}$	σ_h	$\overline{V_d}$	$\overline{C_T}$	1
0.1	0	0	2.351×10^{-1}	1.590×10^{-1}	-2.332×10^{-1}	0	0	1.493×10^{-1}	1.621×10^{-1}	-1.483×10^{-1}
0.25	0	0	1.368×10^{-1}	1.642×10^{-1}	-1.358×10^{-1}	0	0	1.462×10^{-1}	1.654×10^{-1}	-1.454×10^{-1}
0.4	0	0	1.254×10^{-1}	1.653×10^{-1}	-1.247×10^{-1}	0	0	1.454×10^{-1}	1.673×10^{-1}	-1.446×10^{-1}
0.55	0	0	1.274×10^{-1}	1.635×10^{-1}	-1.267×10^{-1}	0	0	1.465×10^{-1}	1.683×10^{-1}	-1.457×10^{-1}
0.70	0	0	1.314×10^{-1}	1.623×10^{-1}	-1.307×10^{-1}	0	0	1.443×10^{-1}	1.682×10^{-1}	-1.435×10^{-1}
0.85	0	0	1.359×10^{-1}	1.620×10^{-1}	-1.352×10^{-1}	0	0	1.446×10^{-1}	1.686×10^{-1}	-1.439×10^{-1}
1.00	0	0	-4.463×10^{-6}	1.556×10^{-1}	1.287×10^{-3}	0	0	-3.427×10^{-6}	1.576×10^{-1}	1.199×10^{-3}